

Theory of finite strain superplasticity

Miguel Lagos*

Facultad de Ingeniería, Universidad de Talca, Campus Los Niches, Curicó, Chile

César Retamal

*Facultad de Ingeniería, Universidad de Talca, Campus Los Niches, Curicó, Chile and
Université de Paris X–Nanterre, 200 Avenue de la République, 9200 NANTERRE Cedex, France*

(Dated: November 14, 2009)

The plastic flow of a polycrystal is analyzed assuming grains as fine that the rate limiting process is grain boundary sliding, and grains readily accommodate their shapes by slip to preserve spatial continuity. It is shown that thinking of a polycrystal with randomly oriented grains as an homogeneous and isotropic continuum when dealing with it as a dynamical medium, even in a scale much larger than the grain size, leads to gross errors. The polyhedral nature of grains influences the plastic flow in a radical manner, as the relative velocity of adjacent grains is constrained to the common boundary plane, and only the in-plane shear stress contributes to their relative motion. This constriction determines that $\nabla \cdot \vec{v} \neq 0$, where \vec{v} is the velocity field of the material medium, and plastic deformation necessarily involves grain volume variations, which can only be elastic. As this has a limit, fracture follows as a necessary step of plastic flow. A theoretical approach to plastic flow is developed, and emphasis is done in superplastic deformation, from zero to fracture strain. The theory allows to quantitatively explain the observed features of superplastic materials and responds to many open questions in the field.

PACS numbers: 62.20.fg, 46.35.+z, 62.20.mj, 62.20.mm

I. INTRODUCTION

Superplasticity is an anomalously high tensile ductility occurring in a growing class of fine grained polycrystalline solids. At rather precise conditions of composition, grain refinement, temperature and strain rate, they can undergo uniform neckless plastic elongations that may reach thousands of percent prior to fracture. These large strains occur with no significant change in the grain shapes or sizes, nor in any other fine attribute [1, 2]. As well, different bodies in the superplastic regime of deformation become prone to diffuse one into the other when their surfaces make contact (diffusion bonding). Among the many singular features of the phenomenon is the fairly narrow range of temperatures over which it happens. For instance, tensile tests for the superplastic titanium alloy Ti-6Al-4V give maximum ductility at temperatures close to 1153 K, and elongation to fracture rapidly decays to half the optimal figure within a neighborhood not wider than 200 K around [3]. These temperatures are well below the melting point (1930 K), so we are talking about a genuine solid state effect.

Beside the scientific problem it poses, superplasticity has acquired considerable technical importance. After the pioneer work of Backofen on the superplastic forming of Zn-Al sheets by a simple air pressure operation [4], as in the fabrication of plastic bottles, and the discovery of a number of high strength superplastic alloys, the subject moved into the scope of engineering materials for ad-

vanced applications. Since then, the list of high strength superplastic alloys, intermetallic compounds and ceramics has increased notably [2], together with the technical knowledge for producing superplastic structures. A number of present day aluminium superplastic alloys, like Al-7475, Al-8090 and Supral 220, or titanium Ti-6Al-4V and SP700, have outstanding importance as aeronautic materials [5]. Superplastic forming combined with diffusion bonding is now a standard technique for producing both engine and airplane structural parts. The development of light ductile materials of high strength at elevated temperatures has a principal role in the race for more efficient aeroengines. Superplastic titanium and nickel aluminides are drawing great attention in this respect [2, 5]. Having half the density of the current materials, TiAl-based alloys are promising candidates to replace the nickel-based superalloys in combustion chambers and turbine blades.

After a large plastic deformation with no significant microstructural changes, and resembling a steady flow, superplastic solids collapse at a rather well-defined strain, which depends on temperature and strain rate. The regular behaviour of superplastic elongation to fracture suggests that the phenomenon is governed by a specific variable, not identified so far, which keeps account for the total strain and produces failure when reaching a precise value. Certainly, the development of cavities may contribute to precipitate collapse [6, 7] but seems not to be the main cause. Maximum elongation to fracture strongly depends on the strain rate, while the evolution of cavities, when occurring, has been observed to be almost independent of that variable [8, 9]. Moreover, titanium superplastic alloys do not cavitate significantly [3, 10].

For decades, people have been interpreting their ob-

*Electronic address: mlagos@utalca.cl

servations on the basis of constitutive equations of the form $\sigma^n = \dot{\epsilon}^m/A$, relating the uniaxial applied stress σ with the superplastic strain rate $\dot{\epsilon}$. The coefficient A depends on the microstructure and follows an Arrhenius dependence with temperature. A variety of theories give this kind of equation with constant m , [11, 12, 13, 14, 15, 16, 17, 18]. Nevertheless, experiments show that $\log \sigma$ and $\log \dot{\epsilon}$ are never linearly related, as implied by the power law, but the curves display a sigmoidal shape, which is a characteristic feature of the superplastic deformation, and the value of the strain rate sensitivity m that fits the data near the inflexion point is usually a non-integral number which vary strongly with strain rate and strain. In many superplastic materials the large ductility is observed even for $\log \dot{\epsilon}$ far from the inflexion point, where the slope m has changed, and the strain rate at the inflexion point shifts considerably with strain [19].

Despite the success of some previous work in accurately predicting the temperature dependent stress *vs.* strain rate curves at zero or small strain for a number of superplastic solids [20, 21, 22], it rests to explain why are they superplastic. Knowing the mechanisms that make the grains to slide past each other and the successful prediction of plastic properties at small strains are not enough to answer this question, and it is necessary to investigate how grains flow over long paths when the solid undergoes a finite deformation. The literature shows several different theoretical attempts to explain superplastic phenomena, but no one addresses the point of the modifications occurring inside the material when strained up to fracture [11, 12, 13, 14, 15, 16, 17, 18, 20, 21, 22], and the dependence of the stress *vs.* strain rate curves with strain.

We put forward here a general theoretical approach for the plastic deformation of fine grained solids up to fracture strain. We assume the grain boundary sliding mechanisms of Refs. 21 and 22, but refine the study of the grain collective motions in the spirit of Ref. 23. The latter is also modified in order to interpret better the physics of the sliding grains. As a general conclusion, our results prove that the deformation and fracture properties of superplastic solids are governed by general laws amenable of analytical mathematical description, simple and accurate enough to constitute a practical tool for interpreting material tests. Though the assorted conglomerate of possible structural defects may affect in specific situations, the main mechanical behaviour of solids is determined by a few parameters associated to the most basic structural properties.

II. STRESS TENSOR AND PLASTIC STRAIN RATES

A. General considerations

At a scale much larger than the grain size, polycrystalline matter lacks symmetry constrictions and periodicity, and displays same average packing and properties in all directions, and over its whole extension. However, despite this, assimilating a polycrystal to an homogeneous and isotropic continuum may lead to gross errors, no matter the scale, when dealing with it as a dynamical medium. It has been proven before [23], and is revised in this section, that the faceted nature of the structural constituents of a polycrystal, the grains, influences the macroscopic plastic flow in a radical manner.

To explain briefly how this does happen, assume that plastic flow takes place by just grain sliding, and that grains readily accomodate their shapes by slip, so the rate limiting process is the former. Sliding of two adjacent grains occurs when the shear stress in the plane of the common boundary exceeds a critical value τ_c . However, no matter how big the externally applied forces may be, shear stresses vanish in planes whose normals are in the principal directions of the stress tensor. By continuity, shear stresses in planes whose normals are inside well-defined finite solid angles around the principal directions are smaller than τ_c . Hence, many grains are impeded to slide simply because of the orientation of their surfaces [23]. By this effect, the material medium ceases to be dynamically isotropic, and cones are created by the very external forces within which no displacement is allowed. These forbidden cones destroy the kinematic balance and $\nabla \cdot \vec{v} \neq 0$, where \vec{v} represents the velocity field of the flowing medium. Hence, mass density is not locally conserved in the overall plastic flow. The consequent internal pressure build up helps deformation and, at a critical strain, the material becomes mechanically unstable, undergoing brittle or ductile fracture, depending on the precise physical circumstances. The internal pressure p , which operates in the local microscopic scale, keeps account of cumulated strain and triggers fracture at a precise value of it.

B. Relative velocities between adjacent grains and strain rates

The proper configuration variables in the macroscopic scale are the components ε_{ij} ($i, j = x, y, z$) of the strain tensor, which, together with their time derivatives $\dot{\varepsilon}_{ij}$, give a complete picture of the dynamical state of the system. However, the evolution of ε_{ij} in time is governed by forces exerted between each pair of adjacent grains, and hence the dynamical analysis demands to go first to the grain level. As the objective is to return to the larger scale, the first task is to establish the connection between the two descriptions.

Given the statistics of spatial orientations of the grain boundaries, which may be assumed isotropic from the beginning, one can derive the relation between $\dot{\epsilon}_{ij}$ and the set of the relative velocities $\Delta\vec{v}$ between pairs of adjacent grains. To show this, temporarily place the origin O of the coordinate system at a point of a grain surface. Then call \vec{v} the velocity of a point P in the positive i -coordinate axis, which is in another grain boundary distant $x_i = nd$ from O, where n is a large natural number and d the mean grain size. (In what follows it will be denoted either $i, j = x, y, z$ or $i, j = 1, 2, 3$, with $x_1 \equiv x, x_2 \equiv y, x_3 \equiv z$).

As there are n contiguous grains between points O and P, \vec{v} is the sum

$$\vec{v} = \sum_{p=1}^n \Delta\vec{v}(p) + \sum_{p=1}^n u_i(p)\hat{e}_i, \quad (1)$$

where p correlatively numbers the adjacent grains along the i -axis and $\Delta\vec{v}(p)$ is the velocity of grain p relative to grain $p-1$ at the interface between them. The second term in the right hand side of Eq. (1) accounts for the assumed deformability of the grains, \hat{e}_i is the unit vector along the i -axis and $u_i(p)$ stands for the expansion rate of grain p along the i -direction. However, we are considering plastic deformation processes in which grains remain equiaxed in the mean and do not vary significantly their average size. Therefore, on this basis, as n is large we can set

$$\sum_{p=1}^n u_i(p)\hat{e}_i = 0, \quad (2)$$

which means that, statistically speaking, the grains neither stretch nor shrink. Hence

$$\vec{v} = \sum_{p=1}^n \Delta\vec{v}(p). \quad (3)$$

If the solid is being deformed, the components of the displacement of P in a time δt are

$$v_i\delta t = \dot{\epsilon}_{ii}x_i\delta t, \quad v_j\delta t = \dot{\epsilon}_{ji}x_i\delta t \quad (j \neq i). \quad (4)$$

Substituting $x_i = nd$ and Eq. (3) in Eqs. (4), it is obtained that

$$\dot{\epsilon}_{ji} = \frac{1}{nd} \sum_{p=1}^n \Delta v_j(p), \quad (5)$$

where the i dependence in the right hand side is implicit in the direction along which the relative velocities are sampled. (Notice that the present arguments leading to Eq. (5) do not assume that the grains are rigid, as seems

implicit in the demonstration given in Ref. 23, but that they conserve mean size and shape in the plastic flow).

If the material is homogeneous and isotropic in the macroscopic scale, the n plane grain interfaces intersecting OP are oriented in any direction with the same probability. Therefore, one may interpret the sum in Eq. (5) as an average which, as n is large, runs over all possible orientations of the grain boundaries intersecting OP. However, vectors $\Delta\vec{v}$ represent relative velocities between consecutive grains ordered along the positive i -coordinate axis. Thus, to take this into account, the average must be performed over all orientations in the hemisphere $x_i \geq 0$. Equivalently, denoting \hat{n} the unit vector normal to the interface between two grains, the sum in Eq. (5) can be replaced by an integral over all directions \hat{n} satisfying the condition $\hat{n} \cdot \hat{e}_i \geq 0$. Therefore, we can write

$$\dot{\epsilon}_{ij} = \frac{1}{d} \langle \Delta v_j \rangle_i, \quad (6)$$

where symbol $\langle \dots \rangle_i$ means the average over all orientations in the semispace $x_i \geq 0$. If the material is not isotropic in the larger scale, for instance because the grains are not equiaxed, the average (6) should incorporate the proper weight factors.

C. Relative velocities between adjacent grains and stresses

The stress tensor

$$(\sigma_{ij}) = \begin{pmatrix} \sigma_x & 0 & 0 \\ 0 & \sigma_y & 0 \\ 0 & 0 & \sigma_z \end{pmatrix}, \quad (7)$$

is diagonal in the main frame of reference (xyz) , with σ_i ($i = x, y, z$) being the principal stresses. To properly express the physics at the grain scale, define a local frame of reference $(x'y'z')$ whose $x'y'$ plane is in the common grain boundary plane of two adjacent grains (Fig. 1). In the local reference system the stress tensor reads

$$(\sigma_{i'j'}) = R(\sigma_{ij})R^T, \quad (8)$$

where R is the rotation matrix that makes the transformation from the (xyz) to the $(x'y'z')$ frames, and R^T is the transposed of R .

As pointed out in Ref. 21, superplastic grain boundary sliding seems closely related with elastic instabilities occurring at interfaces in solids when subjected to overcritical stresses [24, 25, 26, 27, 28, 29, 30, 31, 32, 33]. Monte Carlo simulation and analytical treatment show that, in general, planar structures inside the bulk of crystalline matter become rough when subjected to high enough in-plane shear forces [24]. After the occurrence of the elastic instability the locally induced normal stress field drives

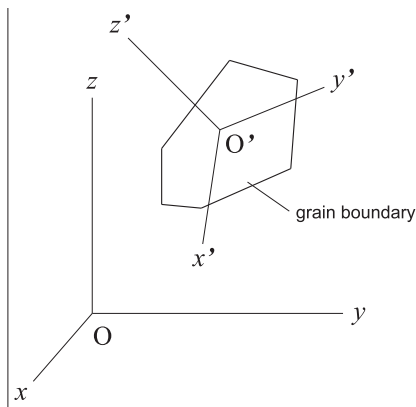


FIG. 1: Local reference system $(x'y'z')$, with the z' axis normal to the plane of the common boundary of two adjacent grains. The axes of the (xyz) frame of reference are in the principal directions of the stress tensor.

an active atomic transport between the interface and the two adjacent crystals. This bulk effect is closely related with the Asaro–Tiller–Grinfeld instability, *i. e.* stress induced roughening of solid surfaces [25, 26, 27], and with the spontaneous roughening of thin films produced by strong in-plane stresses arising from lattice mismatch with the substrate [28, 29, 30, 31, 32, 33].

It has been shown that the active atomic transport between the buckled grain boundary and the two adjacent grains follows closed paths, which makes the two grain surfaces to slide [21]. The relative velocity between the two sliding grains turns out to be proportional to the in-plane components, $\sigma_{x'z'}$ and $\sigma_{y'z'}$, of the shear stress operating in the shared grain boundary plane, provided that the total in-plane shear stress

$$\tau_{z'} = \sqrt{\sigma_{x'z'}^2 + \sigma_{y'z'}^2} \quad (9)$$

be higher than the threshold stress τ_c for the elastic instability of the grain boundary [21, 22, 23]. Hence

$$\Delta v_{i'} = \begin{cases} \mathcal{Q} \sigma_{i'z'} \left(1 - \frac{\tau_c}{\tau_{(x'y')}}\right), & \text{if } \tau_{(x'y')} > \tau_c, \quad i' = x', y', \\ 0, & \text{otherwise,} \end{cases} \quad (10)$$

$$\Delta v_{z'} \equiv 0,$$

where \mathcal{Q} is a coefficient depending on the normal stresses $\sigma_{i'i'}$ which will be discussed in detail in the next section. The factor $(1 - \tau_c/\tau_{z'})$ ensures that $\Delta \vec{v} = 0$ for $\tau_{z'} = \tau_c$.

The coefficient \mathcal{Q} must not depend on the orientation of the local frame of reference $(x'y'z')$, therefore its dependence on the normal stresses is only via the invariant

$$p = -\frac{1}{3}(\sigma_{x'x'} + \sigma_{y'y'} + \sigma_{z'z'}) = -\frac{1}{3}(\sigma_x + \sigma_y + \sigma_z). \quad (11)$$

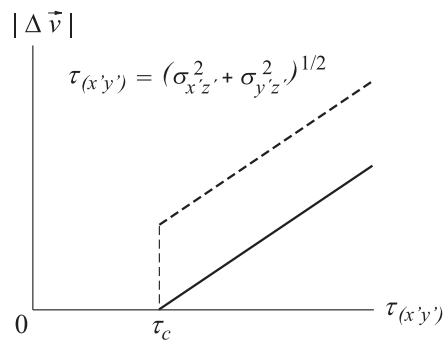


FIG. 2: The solid line represents the linear relation assumed here between $|\Delta \vec{v}|$ and the total in-plane shear stress. The dotted line represents the model of Ref. [23].

This is also a necessary and sufficient condition for considering $\mathcal{Q}(p)$ as independent of the shear stresses for any orientation of the grain boundary. But for the critical condition incorporated in Eqs. (10), \mathcal{Q} may be seen as an inverse grain boundary viscosity coefficient [15, 34, 35].

Notice that $\Delta v_{i'}$ in Eqs. (10) is related with an irreversible shift between the two grains, and hence cannot describe the variation of an elastic degree of freedom. In what follows, elastic and plastic strains will be independent mechanical variables (which nevertheless do interact). Grain elastic distortions are always implicit in the subsequent developments, but plastic strains are the dynamical variables because grains are the flowing entities. Elastic strains of the grains will remain implicit in the stresses, which are linearly related with elastic strains through the equations of the theory of elasticity.

To put Eqs. (10) in a more practical way, we must perform the matrix transformation (8), choose the proper components of $(\sigma_{i'j'})$ to insert them in Eqs. (10) and write $\Delta \vec{v}$ in the local $(x'y'z')$ reference system, and then make the inverse vector transformation to express $\Delta \vec{v}$ in the main (xyz) coordinate system. Hence, for $\tau_{z'} > \tau_c$ the components $\Delta v_{i'}$ are

$$\Delta v_{i'} = \mathcal{Q} [R(\sigma_{ij})R^T]_{i'z'} \left(1 - \frac{\tau_c}{\tau_{(x'y')}}\right), \quad i' = x', y',$$

$$\Delta v_{z'} = 0, \quad (12)$$

where $[\dots]_{i'z'}$ selects the $i'z'$ component of the tensor. When expressed in the (xyz) frame, the relative velocities (12) are $(\Delta v_i) = R^T(\Delta v_{i'})$ or, more explicitly,

$$\Delta v_i = \sum_{i'=x',y'} R_{i'i} \Delta v_{i'}, \quad i = x, y, z. \quad (13)$$

The local $(x'y'z')$ frame can be arbitrarily rotated around the z' axis without breaking the condition that z' be normal to the grain boundary plane. Then, the x' axis can always be chosen on the xy plane, as in Fig. 3.

Calling ϕ the Euler angle between the x' and x axes, and θ the other Euler angle, going from the z to the z' axis, the rotation matrix reads

$$R(\theta, \phi) = \begin{pmatrix} \cos \phi & \sin \phi & 0 \\ -\sin \phi \cos \theta & \cos \phi \cos \theta & \sin \theta \\ \sin \phi \sin \theta & -\cos \phi \sin \theta & \cos \theta \end{pmatrix}. \quad (14)$$

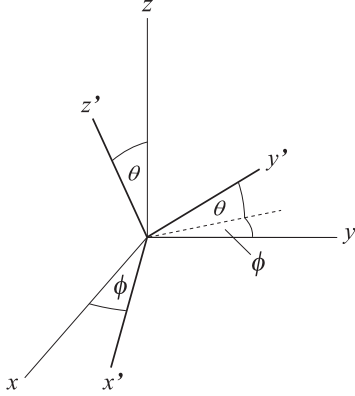


FIG. 3: Angles between the axes of the local reference system ($x'y'z'$) and the principal directions. The x' axis is in the xy plane.

Transforming (σ_{ij}) with the matrix (14) one obtains, in particular, that

$$\begin{aligned} \sigma_{x'y'} &= (\sigma_x - \sigma_y) \sin \phi \cos \phi \sin \theta \\ \sigma_{y'z'} &= -(\sigma_x \sin^2 \phi + \sigma_y \cos^2 \phi - \sigma_z) \sin \theta \cos \theta, \end{aligned} \quad (15)$$

and, making the inverse vector transformation (13), the components of the relative velocity between grains takes the explicit form

$$\begin{aligned} \Delta v_x &= \mathcal{Q} \sin \theta [(\sigma_x - \sigma_y) \sin \phi \cos^2 \phi + (\sigma_x \sin^2 \phi \\ &\quad + \sigma_y \cos^2 \phi - \sigma_z) \sin \phi \cos^2 \theta] \left(1 - \frac{\tau_c}{\tau(\theta, \phi)}\right) \\ \Delta v_y &= \mathcal{Q} \sin \theta [(\sigma_x - \sigma_y) \sin^2 \phi \cos \phi - (\sigma_x \sin^2 \phi \\ &\quad + \sigma_y \cos^2 \phi - \sigma_z) \cos \phi \cos^2 \theta] \left(1 - \frac{\tau_c}{\tau(\theta, \phi)}\right) \\ \Delta v_z &= -\mathcal{Q}(\sigma_x \sin^2 \phi \\ &\quad + \sigma_y \cos^2 \phi - \sigma_z) \sin^2 \theta \cos \theta \left(1 - \frac{\tau_c}{\tau(\theta, \phi)}\right). \end{aligned} \quad (16)$$

Eqs. (16) hold when

$$\tau(\theta, \phi) > \tau_c, \quad (17)$$

with

$$\begin{aligned} \tau(\theta, \phi) &= [(\sigma_x - \sigma_y)^2 \sin^2 \phi \cos^2 \phi \sin^2 \theta \\ &\quad + (\sigma_x \sin^2 \phi + \sigma_y \cos^2 \phi - \sigma_z)^2 \sin^2 \theta \cos^2 \theta]^{1/2}, \end{aligned} \quad (18)$$

otherwise $\Delta \vec{v} = 0$.

D. Strain rates and stresses

To simplify the equations, let us particularize to the important case of uniaxial external stress σ_z . Far from the sample surfaces, the material has cylindrical symmetry and $\sigma_x = \sigma_y$, which will be assumed not to vanish for the sake of generality. Eqs. (16) and (18) greatly reduce and give

$$\begin{aligned} \Delta \vec{v} &= \mathcal{Q}(\sigma_z - \sigma_x) \sin \theta \cos \theta \\ &\quad \times \left(1 - \frac{\tau_c}{|(\sigma_z - \sigma_x) \sin \theta \cos \theta|}\right) \hat{v} \quad (\sigma_x = \sigma_y), \end{aligned} \quad (19)$$

where the unit vector \hat{v} in the (x, y, z) system is

$$\hat{v} = (-\sin \phi \cos \theta, \cos \phi \cos \theta, \sin \theta). \quad (20)$$

The choice of the x' axis in the xy plane proves to be particularly convenient because, by the cylindrical symmetry, any direction in the xy plane is a principal direction, and then $\sigma_{x'z'} = 0$ for any θ and ϕ . The condition (17) on the minimal shear stress τ_c becomes

$$|(\sigma_z - \sigma_x) \sin \theta \cos \theta| > \tau_c, \quad (\sigma_x = \sigma_y), \quad (21)$$

which determines a critical angle θ_c , given by

$$\sin(2\theta_c) = \frac{2\tau_c}{|\sigma_z - \sigma_x|}, \quad (22)$$

such that $\Delta \vec{v} \equiv 0$ for $|\sin 2\theta| < \sin 2\theta_c$. Therefore, under the restriction that $\sigma_x = \sigma_y$, plastic flow is not allowed for $0 \leq \theta < \theta_c$, $\pi/2 - \theta_c < \theta < \pi/2 + \theta_c$ and $\pi - \theta_c < \theta < \pi$, as shown in Fig. 4(a).

To calculate the averages $\langle \Delta v_j \rangle_i$, appearing in Eq. (6), we must integrate over all directions (θ, ϕ) such that the unit vector $\hat{n}(\theta, \phi)$, normal to the grain boundary plane, has positive projection on the x_i axis. Vector \hat{n} is the unit vector \hat{k}' along the z' axis of the local coordinate system, that is,

$$\hat{n} = (\sin \phi \sin \theta, -\cos \phi \sin \theta, \cos \theta). \quad (23)$$

In general,

$$\langle \Delta \vec{v} \rangle_i = \frac{1}{2\pi} \int_{D_i} d\phi d\theta \sin \theta \Delta \vec{v}(\theta, \phi), \quad (24)$$

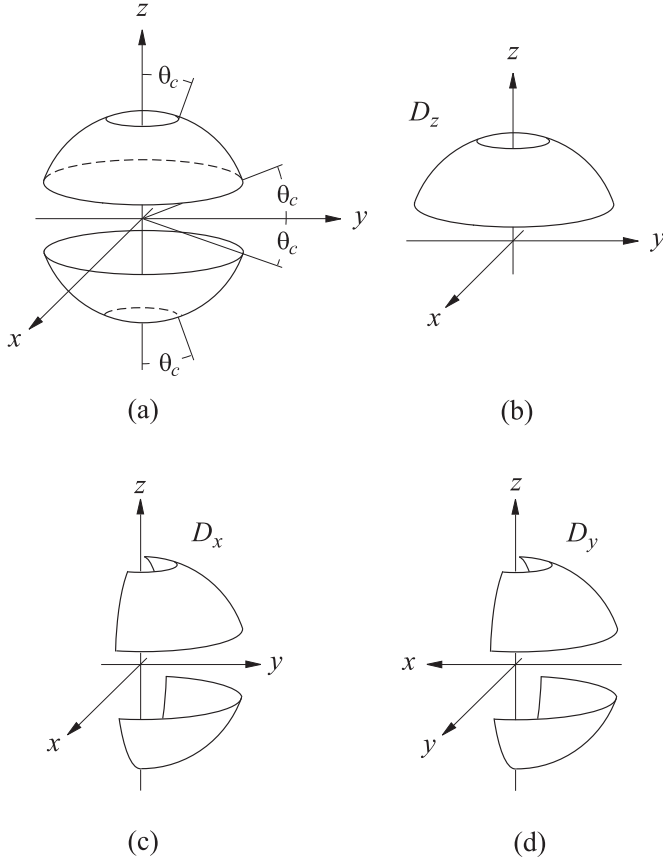


FIG. 4: (a) Grain boundaries whose normals are in the spherical shells are the only ones allowed to slide, if the stress field has cylindrical symmetry with respect to the z axis. Grain boundaries whose normals make angles $0 \leq \theta < \theta_c$, $\pi/2 - \theta_c < \theta < \pi/2 + \theta_c$ and $\pi - \theta_c < \theta < \pi$ with the z axis do not contribute to plastic flow. (b), (c) and (d) Integration domains for integral (24).

and the integration domains D_i can be determined by examining the geometry of the $(xyz) \rightarrow (x'y'z')$ transformation. They are (Fig. 4(b),(c) and (d))

$$\begin{aligned}
 D_x : \theta &\in [\theta_c, \pi/2 - \theta_c] \cup [\pi/2 + \theta_c, \pi - \theta_c], \\
 \phi &\in [0, \pi], \\
 D_y : \theta &\in [\theta_c, \pi/2 - \theta_c] \cup [\pi/2 + \theta_c, \pi - \theta_c], \\
 \phi &\in [\pi/2, 3\pi/2], \\
 D_z : \theta &\in [\theta_c, \pi/2 - \theta_c], \\
 \phi &\in [0, 2\pi].
 \end{aligned} \tag{25}$$

Integrating and combining with Eq. (6) one obtains

$$\dot{\epsilon}_{zz} = \frac{\mathcal{Q}}{4d} [(\sigma_z - \sigma_x) \cos(2\theta_c) - \tau_c(\pi - 4\theta_c)], \tag{26}$$

and

$$\begin{aligned}
 \dot{\epsilon}_{xx} = \dot{\epsilon}_{yy} = &-\frac{\mathcal{Q}}{8d}(\sigma_z - \sigma_x) \left[1 - \frac{4\theta_c}{\pi} + \frac{\sin(4\theta_c)}{\pi} \right] \\
 &+ \frac{\mathcal{Q}\tau_c}{\pi d} \cos(2\theta_c).
 \end{aligned} \tag{27}$$

Eqs. (26) and (27) hold for $\sigma_z - \sigma_x > 0$. When $\sigma_z - \sigma_x < 0$ they must be modified reversing the sign of the terms multiplied by τ_c .

By Eq. (22), $\sigma_z - \sigma_x$ can be written in terms of just θ_c and the constant τ_c . Replacing in Eqs. (26) and (27), the strain rates turn out to be entirely determined by θ_c , which becomes a natural and convenient auxiliary variable which varies in the range

$$0 \leq \theta_c \leq \pi/4. \tag{28}$$

For finite τ_c , $\theta_c = 0$ corresponds to the asymptotic situation in which the external forces applied on the sample are very strong. For $\theta_c = \pi/4$, the forbidden directions extend over the whole sphere and no grain is allowed to slide.

As the relative velocities, the strains ϵ_{ij} are purely plastic, but elastic strains are not disregarded and remain implicit in the stresses, which are linearly related with elastic strains through the equations of the theory of elasticity.

III. DILATION RATE AND INTERNAL PRESSURE BUILD UP

From Eqs. (26) and (27), the dilation rate $\dot{V}/V = \dot{\epsilon}_{xx} + \dot{\epsilon}_{yy} + \dot{\epsilon}_{zz}$ turns out to be

$$\begin{aligned}
 \frac{\dot{V}}{V} = &-\frac{\mathcal{Q}}{4d}(\sigma_z - \sigma_x) \left[1 - \cos(2\theta_c) - \frac{4\theta_c}{\pi} \right. \\
 &\left. - \frac{\sin(4\theta_c)}{\pi} + \left(\frac{\pi}{2} - 2\theta_c \right) \sin(2\theta_c) \right],
 \end{aligned} \tag{29}$$

where V stands for the volume of the sample.

Eq. (29) discloses the amazing feature that the dilation rate does not vanish in general if the threshold stress for grain boundary sliding $\tau_c \neq 0$. If $\tau_c = 0$ Eqs. (26) and (27) reduce to

$$\begin{aligned}
 \dot{\epsilon}_{zz} &= \frac{\mathcal{Q}}{4d}(\sigma_z - \sigma_x), \\
 \dot{\epsilon}_{xx} = \dot{\epsilon}_{yy} &= -\frac{\mathcal{Q}}{8d}(\sigma_z - \sigma_x) \quad (\tau_c = 0),
 \end{aligned} \tag{30}$$

$\dot{V}/V = 0$ and the material flows as a viscous liquid.

The dilation rate (29) vanishes only in the extreme cases $\theta_c = 0$ and $\theta_c = \pi/4$, and for $\sigma_z - \sigma_x > 0$ is negative for any other value in between. This means that

plastic stretching involves a spontaneous compression of the grains, which can only be elastic, and demands the ability of the material to support some elastic volume reduction. As this ability is essentially limited, plastic strain is limited as well, and a finite strain to failure is implicit in Eq. (29). The single-crystal elastic compressibility will determine how much the polycrystal could be plastically elongated.

Another general consequence of Eq. (29) is that, in general, the transversal stresses $\sigma_x = \sigma_y$ do not vanish in the plastic deformation, even when the applied external force is strictly uniaxial, and the material is isotropic in a scale much larger than the grain size. This may seem rather odd if one has in mind a static, or quasistatic, picture of the deformation process. Such a picture is, however, misleading. Plastic flow is an essentially dynamic process.

It must be noted that Eq. (29) deals with volume changes, which are necessarily elastic, but has nothing to do with grain shape variations. Our primary hypothesis is that grains are plastic, and they readily accommodate their shapes to preserve matter continuity, but grain boundary sliding is the rate limiting process. This is consistent with accommodation by slip, since crystal deformation by slip does not demand much additional stress once the critical resolved shear stress (CRSS) has been exceeded. Then, if τ_c is greater than the CRSS of the material then our hypothesis about grain plasticity should hold. We are not very specific about the accommodation mechanisms because grain plastic deformation is not the rate limiting process, diffusional creep or dislocation creep may contribute, but we assume that the main accommodation mechanism is by slip processes.

Settling $\sigma_x = \sigma_y = 0$ for $\varepsilon_{zz} = 0$ is a natural initial condition. However, it will be shown that, as the plastic stretching along the z axis increases with time, the magnitude of the transversal stresses $\sigma_x = \sigma_y$ monotonically increases as well, with negative sign. Hence, the plastic elongation of the sample produces a spontaneous compression in the transversal plane. Neck formation prior to ductile fracture of polycrystalline bars can be attributed to this circumstance.

The dilation rate (29) can be understood in a qualitative manner by a simple geometric argument. The relative speed $|\Delta\vec{v}|$ between adjacent grains depends only on θ and is symmetric with respect to $\theta = \pi/4$ in the top hemisphere, and with respect to $\theta = 3\pi/4$ in the bottom one (Eq. (19)). Fig. 5 depicts the solid angles A, B and C in which $\Delta\vec{v} \equiv 0$. Grain boundaries whose normals \hat{n} are in B correspond to banned relative velocities $\Delta\vec{v}$ in A or C, and vice-versa. As the solid angle B is larger than the sum of A and C, there are more suppressed vectors $\Delta\vec{v}$ in A and C than in B. Therefore, grain displacements in the z direction, or close to it, are less favoured than those occurring in directions near the xy plane. If no dilation takes place when $\theta_c = 0$ (i. e. $\tau_c = 0$), some volume change should occur for $\tau_c \neq 0$. The same kind of argument serves to show that no dilation does occur in

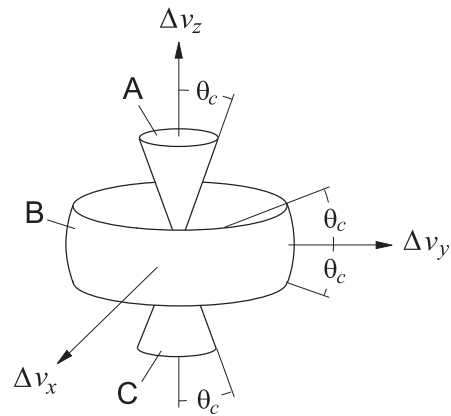


FIG. 5: The forbidden directions for $\Delta\vec{v}$. Vectors $\Delta\vec{v}$ in the solid angles A and C correspond to grain boundaries with \hat{n} in the solid angle B, and vice-versa. Then, there are more vectors suppressed in A and C than in B.

two dimensions, and the area is conserved in the plastic distortion of a strictly two-dimensional layer.

We will examine the case of the uniaxial plastic strain of a bulk sample along the z axis at a strain rate $\dot{\varepsilon} \equiv \dot{\varepsilon}_{zz}$. The only externally applied stress is $\sigma \equiv \sigma_z$. We will denote also $p = -(\sigma_x + \sigma_y + \sigma_z)/3$ for the pressure. The transversal stresses $\sigma_x = \sigma_y$ are assumed finite to give a chance for internal stresses to develop. Of course, cylindrical symmetry demands that the point into consideration be far enough from the surfaces. With this notation

$$\sigma_x = \sigma_y = -\frac{1}{2}(\sigma + 3p), \quad \sigma_z - \sigma_x = \frac{3}{2}(\sigma + p). \quad (31)$$

Recalling Hooke's law

$$\frac{\Delta V}{V} = -\frac{1}{B} p, \quad (32)$$

where B is the bulk elastic modulus, the dilation rate reads

$$\frac{\dot{V}}{V} = -\frac{1}{B} \frac{dp}{dt}. \quad (33)$$

Replacing the identity $\dot{\varepsilon} dp/d\varepsilon = dp/dt$ and Eq. (29) in Eq. (33),

$$\frac{dp}{d\varepsilon} = s_Q \frac{B\tau_c}{2d\dot{\varepsilon}} \left[\frac{1 - \cos(2\theta_c)}{\sin(2\theta_c)} - 2\theta_c \left(1 + \frac{2}{\pi \sin(2\theta_c)} \right) - \frac{2 \cos(2\theta_c)}{\pi} + \frac{\pi}{2} \right], \quad (34)$$

where use was made of Eq. (22) to eliminate $\sigma_z - \sigma_x$ and put the right hand side in terms of just θ_c . The factor s is

$$s = \begin{cases} 1, & \text{if } \sigma_z - \sigma_x > 0 \\ -1, & \text{if } \sigma_z - \sigma_x < 0. \end{cases} \quad (35)$$

For traction ($s = 1$), the right hand side of Eq. (34) is positive for $0 \leq \theta_c \leq \pi/4$, and hence the pressure p increases monotonically with strain.

Elastic degrees of freedom, implicit in \dot{V}/V , are brought to the fore once more by Eq. (29). Eq. (33) expresses the volume variation (the trace of the elastic strain rate tensor) in terms of the pressure p (essentially the trace of the stress tensor). Hence it allows to return to the scheme in which the elastic distortions are kept implicit in the stresses. The variation of p in the plastic deformation indicates that elastic and plastic degrees of freedom are coupled.

Written in terms of just the critical angle θ_c , Eq. (26) for the strain rate becomes

$$\dot{\epsilon} = s \mathcal{Q} \frac{\tau_c}{2d} \left[\cot(2\theta_c) + 2\theta_c - \frac{\pi}{2} \right], \quad (36)$$

with

$$\theta_c = \frac{1}{2} \arcsin \left(\frac{4\tau_c}{3|\sigma + p|} \right). \quad (37)$$

In what follows we will consider just traction, and s will be omitted.

At the start of the deformation process $\epsilon = 0$ and $\sigma_x = \sigma_y = 0$. Then the initial condition written in the new notation is

$$p = -\frac{\sigma}{3} \quad \text{for } \epsilon = 0. \quad (38)$$

IV. THE COEFFICIENT \mathcal{Q}

The coefficient \mathcal{Q} , governing grain boundary sliding, was studied in detail in Refs. [21] and [22]. It was shown there that the stress dependence of \mathcal{Q} is only through the pressure p , and varies with temperature and grain size. It obeys the rather simple law

$$\frac{\mathcal{Q}}{4d} = C_0 \frac{\Omega^*}{k_B T} \exp \left(-\frac{\epsilon_0 + \Omega^* p}{k_B T} \right), \quad (39)$$

where k_B is the Boltzmann constant, T the temperature, the coefficient C_0 depends only on the grain size d , the constant ϵ_0 is the energy necessary for evaporating a crystal vacancy from the grain boundary, and Ω^* measures the sensitivity of this energy to stress.

The derivation of expression (39) has been already published [21, 22], but a brief explanation of the physics involved is in order here. The mechanical analysis of a

stressed polycrystalline material must distinguish intergranular and crystalline matter because they have different mechanical properties [21, 22]. A shear stress greater than a critical value applied in the plane of a grain boundary should buckle it, producing either a boundary corrugation or the formation of a periodic series of trenches. This localized deformation induces a periodic normal stress field that alternates compression and traction on the adjacent crystal surfaces, as shown schematically in Fig. 6(a). Grain boundaries are efficient sinks and sources for vacancies and the periodic stress field induced by the buckled boundary yields a periodic variation of the equilibrium value for the concentration of crystal vacancies. The grain boundary then evaporates and condenses the point defects in alternate sectors, producing streams of the defects in closed loops that cross the boundary and involve the two adjacent crystals (Fig. 6(b)). These closed loops perform as the driving pulleys of a conveyor belt and the phenomenon provides either an accommodation mechanism and the driving force for crystal sliding [21, 22].

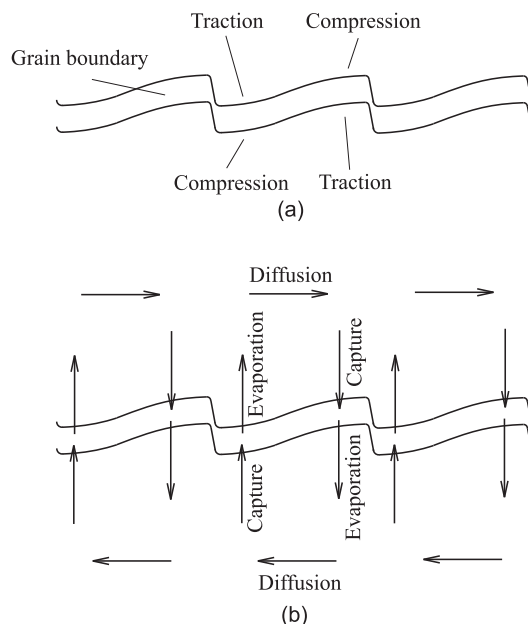


FIG. 6: (a) Schematic representation of a buckled grain boundary, and the induced periodic stress field alternating compression and traction regions in the adjacent crystals. (b) The grain boundary releases and captures crystal vacancies in the tractioned and compressed regions, respectively, producing this way closed paths of the point defects. The diffusion of vacancies, equivalent to an atomic counterflow, have opposite senses in the two grains.

As explained, the grain boundary elastic instability causes a strongly fluctuating stress field, which in the macroscopic scale averages to zero. Be ϵ_B the energy necessary for the grain boundary to release a vacancy

into one of the two crystals adjacent to it, when the system is unstrained. When the grains are strongly stressed, this energy is expected to change linearly with stress, as long as ϵ_B is much larger than its expected variations. Denoting σ_{ij}^1 the characteristic amplitude of the induced stress field spatial fluctuations, the relative concentration of defects in two neighbouring regions of maximal and minimal stress is proportional to

$$\exp\left[-\frac{\epsilon_B + \Omega^*(p + p^1)}{k_B T}\right] - \exp\left[-\frac{\epsilon_B + \Omega^*(p - p^1)}{k_B T}\right], \quad (40)$$

where $p^1 = -(\sigma_{xx}^1 + \sigma_{yy}^1 + \sigma_{zz}^1)/3$ is the contribution from the induced stress field to the pressure. Expression (40) depends only on the normal stresses σ_{xx} , σ_{yy} and σ_{zz} because it is expected that the energy of a vacancy will not be significantly affected by the shear stresses, which do not change the volume of the hole, but only its shape.

The flow of defects between these two regions is proportional to the spatial concentration variation (40), which can be written as

$$D \frac{\Omega^* p^1}{k_B T} \exp\left(-\frac{\epsilon_B + \Omega^* p}{k_B T}\right) \quad (41)$$

for $p^1 \ll p$. In Eq. (41) $D = D_0 \exp[-\epsilon_a/(k_B T)]$ is the diffusion coefficient for crystal vacancies, with ϵ_a being the corresponding activation energy. No matter the details of the process, one can expect that the speed of the boundary sliding be proportional to the rate at which the assisting vacancies flow along the crystal boundaries, and expression (41) leads to the main Eq. (39) with $\epsilon_0 = \epsilon_B + \epsilon_a$.

By the time, direct experimental evidence was supplied by Vetrano *et al.* [36, 37] for the deformation induced supersaturation of vacancies in the vicinity of many grain boundaries of an Al–Mg–Mn alloy during superplastic deformation. Rapid quenching of the sample while being superplastically deformed revealed the formation of very unstable nano-cavities in a great fraction of the grain boundaries, which rapidly coalesce and disappear on moderate heating. The authors show they start forming after cooling and subsequent mounting of the sample in the transmission electron microscope, and conclude that the cavities provides evidence of a supersaturation of crystal vacancies near the sliding grain boundaries. The defects condense into voids when sliding abruptly ceases, and the just released vacancies are not recaptured by the grain boundaries. Hence grain boundary sliding is associated to the observed vacancy excess, which provides evidence of the capital role of these defects in the deformation process.

Some aspects of the mechanism for grain boundary sliding introduced in Refs. 21 and 22, and reviewed above in a more compact approach, resembles the one put forward earlier by Raj and Ashby [34]. In both the shared grain boundary is taken as a material medium able to

release and capture crystal vacancies, to or from the two grains, causing a relative motion of them. Also, in both theoretical approaches the in-plane shear force induces a strongly varying normal stress field localized in the boundary region and, as a consequence, the less ordered intergrain matter evaporates and condenses vacancies in a periodic series of sources and sinks. The main difference is in the physical nature of the sources and sinks for the point defects. In Refs. 21 and 22 the sources and sinks are originated by the buckling and trenching of the initially plane grain boundary (with eventual steps) by effect of the overcritical shear stress applied to it. Raj and Ashby [34] assume an uneven grain boundary subjected to a shear force. Sources and sinks are caused by the variation of the normal stresses induced in the opposite sides of the permanent grain boundary irregularities.

V. THE CONSTITUTIVE EQUATION FOR SMALL STRAIN

A. The equation

When the plastic distortion just starts, $\epsilon \approx 0$ and holds the initial condition (38), $p = -\sigma/3$. Then

$$\theta_c = \frac{1}{2} \arcsin\left(\frac{2\tau_c}{|\sigma|}\right) \quad (42)$$

and, replacing this and Eq. (39) in Eq. (36),

$$\begin{aligned} \dot{\epsilon} = & 2C_0 \frac{\Omega^* \tau_c}{k_B T} \left[\sqrt{\left(\frac{\sigma}{2\tau_c}\right)^2 - 1} + \arcsin\left(\frac{2\tau_c}{\sigma}\right) - \frac{\pi}{2} \right] \\ & \times \exp\left(-\frac{\epsilon_0 - \Omega^* \sigma/3}{k_B T}\right) \quad (\epsilon \approx 0). \end{aligned} \quad (43)$$

Eq. (43) gives the plastic strain rate $\dot{\epsilon}$ of an axially symmetric sample at temperature T under the action of the uniaxial tensile stress σ . Hence it is the constitutive equation of the material for the established conditions.

The discussion on grain sliding of sections II and III is valid for any polycrystalline solid. Also, there is no reason to think that the grain boundary sliding mechanisms leading to Eq. (39) for the coefficient \mathcal{Q} be exclusive to superplastic grain sliding. Hence, in principle, Eq. (43) is expected to hold for the deformation of any fine grained polycrystalline solid, fine enough to ensure that grain boundary sliding be the rate limiting deformation process.

However, the large amount of experimental data available in the literature on the superplastic materials makes them specially suited for testing Eq. (43). The data for very small strain rates, in the range 10^{-5} to 10^{-3} s^{-1} , are specially valuable because the effect of the critical stress τ_c on the stress-strain rate curves is particularly notorious

in it. Such small strain rates are not usual in tensile tests of normal, not superplastic, materials.

B. Comparison with previous results and with experiment

To appreciate how τ_c affects the strain *vs.* strain rate curves, consider Eq. (43) in the asymptotic limit of very large tensile stress σ , such that $\tau_c/\sigma \rightarrow 0$. The equation reduces to

$$\dot{\epsilon} = C_0 \frac{\Omega^* \sigma}{k_B T} \exp\left(-\frac{\epsilon_0 - \Omega^* \sigma/3}{k_B T}\right) \quad (\epsilon \approx 0, \frac{\tau_c}{\sigma} \approx 0), \quad (44)$$

which is the result given in Ref. 21, in which the effect of the critical stress τ_c discussed in sections II and III was passed over. This produces no significant consequence when comparing the theoretical results with data on alloys having small τ_c , as is the case of the aluminium Al-7475 samples whose mechanical testing was reported by Hamilton [38]. However, the data on the same alloy Al-7475 prepared by Pilling and Ridley [39], aluminium Al-8090 SPF [39] or titanium Ti-6Al-4V [3, 10, 40], do show some disagreement with Eq. (44) for strain rates below 10^{-4} s^{-1} .

As an illustrative example, Fig. 7 shows the excellent fit given by Eq. (43) to the data of Cope *et al.* on Ti-6Al-4V [3, 10, 40] together with the curve representing Eq. (44) with the same values for the parameters. The latter has negative concavity over the whole range of $\dot{\epsilon}$ and does not exhibit the characteristic inflexion point, which is traditionally taken as a distinctive feature of superplasticity. However, both curves become practically the same for $\dot{\epsilon} > 5 \times 10^{-4} \text{ s}^{-1}$.

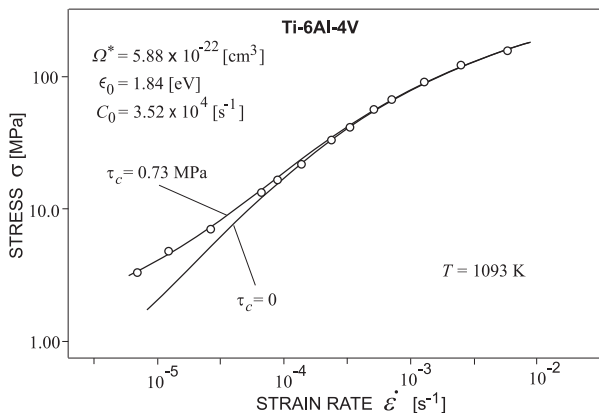


FIG. 7: Curves given by Eqs. (43) and (44), showing the effect of the critical shear stress τ_c . Values for the parameters are shown in the insets. Circles represent data of Cope *et al.*, Refs. 3, 10, 40, on the superplastic titanium alloy Ti-6Al-4V, strained at constant true strain rates and $T = 1093 \text{ K}$.

Figure 7 also illustrates the usefulness of very low strain rate data. As will be seen in the next sections, the

critical shear stress τ_c has important consequences in the plastic deformation at finite strains and high or low strain rates, as fracture, for example, but does not produce any easily recognizable feature in the test curves. On the contrary, at low enough $\dot{\epsilon}$, tensile stresses are close to $2\tau_c$, and the solid angles A, B and C in Fig. 5 have significant magnitudes, producing the inflexion point shown in Fig. 7. As the deformation mechanisms considered here are in principle not exclusive to superplastic materials, we guess that the strain *vs.* strain rate curves for normal ductile materials should exhibit an inflexion point as well, at low enough strain rates.

In a subsequent paper [22], Eq. (44) was modified in the way

$$\dot{\epsilon} = C_0 \frac{\Omega^* (\sigma - \sigma_0)}{k_B T} \exp\left(-\frac{\epsilon_0 - \Omega^* \sigma/3}{k_B T}\right), \quad (45)$$

and an excellent agreement with the experimental results was achieved at low, intermediate and high $\dot{\epsilon}$. However, the introduction of the threshold tensile stress σ_0 was based on just intuitive physical arguments, and justified only by the good results it produced.

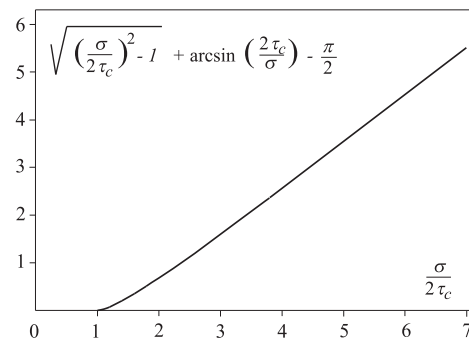


FIG. 8: The pre-exponential factor in Eq. (43) behaves like $\sigma - \sigma_0$ with $\sigma_0 = 2\tau_c$.

Fig. 8 explains the success of Eq. (45). It shows that, despite its more involved appearance, the pre-exponential factor in Eq. (43) is almost linear in σ , and vanishes for $\sigma = 2\tau_c$, which plays the role of σ_0 in Eq. (45). Therefore, Eq. (45) constitutes a very good approximation of the exact Eq. (43), and the same accurate fit of the experimental data on Al-7475, Al-8090 SPF [39], and Ti-6Al-4V [3, 10, 40] attained with the former [22] is to be expected for the latter, but now with no empirically justified modification.

Fig. 9 shows the data of Cope *et al.* [3, 10, 40] on the superplastic titanium alloy Ti-6Al-4V at six temperatures (circles). The solid lines represent Eq. (43). The constants Ω^* , ϵ_0 and C_0 have the same values for the six curves, and are shown in one of the insets. Notice that the values for Ω^* , ϵ_0 and C_0 used here in relation to Eq. (43) are the same than those used in Ref. 22 to insert in Eq. (45), with the same success. The critical shear

stress τ_c evidences some dependence with temperature, as shown in the other inset.

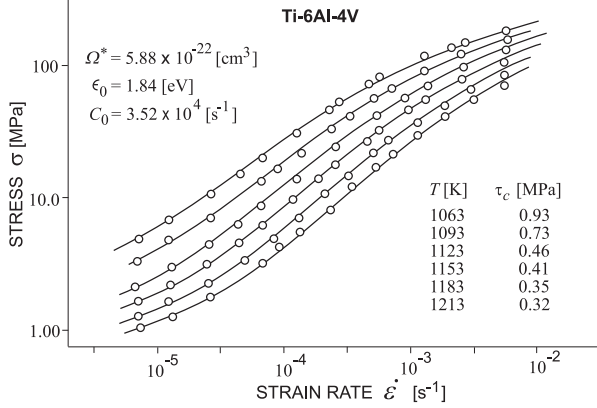


FIG. 9: Stress–strain rate curves for Ti-6Al-4V at six temperatures. Circles represent data of Cope *et al.*, Refs. 3, 10, 40, and solid lines depict Eq. (43) for the parameters shown in the inset. The parameter τ_c exhibits some temperature dependence.

The critical shear stress τ_c is expected to be temperature dependent. It may be equal to either the smaller of the two critical stresses associated to the grain boundary elastic instabilities studied in Refs. 21 and 22, or the critical resolved shear stress (CRSS) of the material when it is greater than the critical stresses for the elastic instabilities. The critical stresses for the elastic instabilities depend on the elastic modulus of the material, which varies with temperature, and the CRSS is temperature dependent as well when the temperature is high enough. For Ti-6Al-4V it seems that τ_c is the CRSS.

VI. FINITE DEFORMATION AT CONSTANT STRAIN RATE

A. The strain function

Deformation up to a finite strain ε can be accomplished in an indefinite number of inequivalent ways because of the other two variables involved in the process, σ and $\dot{\varepsilon}$. Establishing the time dependence of one of them, or its dependence on the intermediate values assumed by ε , would be enough to determine the process. The simplest conditions are to keep $\dot{\varepsilon} = \text{constant}$, as is usually done when testing superplastic materials, or set $\sigma = \text{constant}$, which is the common practice for normal ductile materials. In this section we will assume the former.

Eq. (34) can be put in differential form as

$$d\varepsilon = \frac{2d\dot{\varepsilon}}{B\tau_c} \left(\frac{1 - \cos(2\theta_c)}{\sin(2\theta_c)} - 2\theta_c - \frac{4\theta_c}{\pi \sin(2\theta_c)} - \frac{2 \cos(2\theta_c)}{\pi} + \frac{\pi}{2} \right)^{-1} \frac{dp}{Q(p)}, \quad (46)$$

where $\dot{\varepsilon}$ is considered as a given constant. On the other hand, writing Eq. (36) in the form

$$\frac{2d\dot{\varepsilon}}{\tau_c} \frac{1}{Q} = \cot(2\theta_c) + 2\theta_c - \frac{\pi}{2} \quad (47)$$

and, derivating with respect to p with $\dot{\varepsilon}$ constant, one has that

$$\frac{2d\dot{\varepsilon}}{\tau_c} \frac{1}{Q^2} \frac{dQ}{dp} = \cot^2(2\theta_c) \frac{d\theta_c}{dp}. \quad (48)$$

Derivating also Eq. (39), the alternate expression for dQ/dp

$$\frac{dQ}{dp} = -\frac{\Omega^*}{k_B T} Q \quad (49)$$

is inferred. Replacing it in Eq. (48) and witting the result in differential form gives

$$\frac{dp}{Q} = -\frac{\tau_c k_B T}{d\Omega^* \dot{\varepsilon}} \cot^2(2\theta_c) d\theta_c. \quad (50)$$

Combining Eqs. (46) and (50), and integrating, one finally obtains

$$\varepsilon = -\frac{2k_B T}{B\Omega^*} \int_{\theta_0}^{\theta_c} d\theta \cot^2(2\theta) \left[\frac{1 - \cos(2\theta)}{\sin(2\theta)} - 2\theta - \frac{4\theta}{\pi \sin(2\theta)} - \frac{2 \cos(2\theta)}{\pi} + \frac{\pi}{2} \right]^{-1}, \quad (51)$$

where the limits θ_0 and θ_c correspond to the critical angles for strain $\varepsilon = 0$ and the final value ε of the strain, respectively.

Hence the strain ε is related with the auxiliary variable θ_c by an expression of the form

$$\varepsilon = \frac{k_B T}{B\Omega^*} [F(\theta_c) - F(\theta_0)], \quad (52)$$

where $F(\theta)$ is the universal function

$$F(\theta) = -2 \int d\theta \cot(2\theta) \sin(2\theta) \left[(1 - \cos(2\theta)) - 2\theta \sin(2\theta) - \frac{4\theta}{\pi} - \frac{\sin(4\theta)}{\pi} + \frac{\pi \sin(2\theta)}{2} \right]^{-1}, \quad (53)$$

whose graph is depicted in Fig. 10. $F(\theta)$ is monotonically decreasing in its whole range $(0, \pi/4)$, and diverges at $\theta = 0$ and $\theta = \pi/4$.

The equation for the critical angle θ_0 at $\varepsilon = 0$ follows from combining Eqs. (42) and (43) in order to eliminate σ . It is obtained

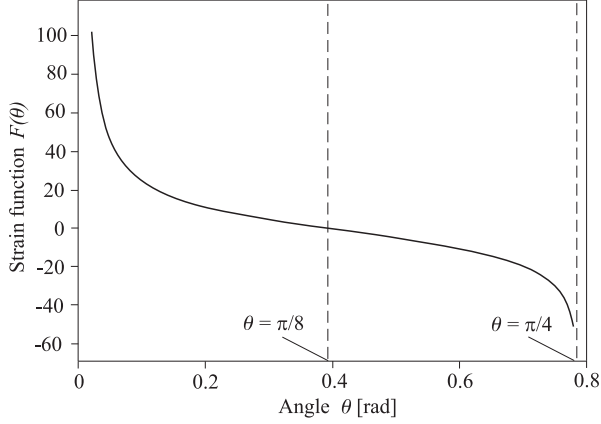


FIG. 10: The strain universal function $F(\theta)$ and its asymptotes at $\theta = 0$ and $\theta = \pi/4$.

$$\dot{\epsilon} = 2C_0 \frac{\Omega^* \tau_c}{k_B T} \left[\cot(2\theta_0) + 2\theta_0 - \frac{\pi}{2} \right] \times \exp \left[-\frac{1}{k_B T} \left(\epsilon_0 - \frac{2\Omega^* \tau_c}{3 \sin(2\theta_0)} \right) \right]. \quad (54)$$

This equation gives θ_0 as a function of $\dot{\epsilon}$ and T . Therefore, the set of Eqs. (52), (53) and (54) allows to determine $\theta_c = \theta_c(\epsilon, \dot{\epsilon}, T)$.

The adimensional coefficient appearing in Eq. (52) establishes the scale for ϵ and is a very small number. The bulk elastic modulus B is close to 0.7×10^{11} Pa for aluminium and 1.0×10^{11} Pa for titanium at normal room temperature. From the comparison of our curves with experiments for $\epsilon \approx 0$, we know that Ω^* is $2.6 \times 10^{-21} \text{ cm}^3$ for Al-8090 and $5.9 \times 10^{-22} \text{ cm}^3$ for Ti-6Al-4V at rather high temperatures, however, Ω^* is not expected to vary with T . Hence, at $T = 300 \text{ K}$,

$$\frac{k_B T}{B \Omega^*} \sim 2.3 \times 10^{-5} - 7.0 \times 10^{-5}. \quad (55)$$

At elevated temperatures, B may decrease substantially, but anyway the coefficient (55) is expected to remain small.

Because of the small value of the coefficient (55), any significative strain ϵ demands that either θ_0 or θ_c , or both, be in one of the two asymptotic regions $\theta \gtrsim 0$ or $\theta \lesssim \pi/4$. The asymptotic region $\theta \lesssim \pi/4$ can be associated to creep, while $\theta \gtrsim 0$ is related to ductile and superplastic deformation. For example, to attain a strain $\epsilon \sim 1 - 10\%$ it must be $F(\theta_c) - F(\theta_0) \sim 1000$. Observing Fig. 10 one readily realizes that such big differences can only exist in the asymptotic regions of $F(\theta)$.

B. The strain and strain rate dependent stresses

Combining Eqs. (36) and (39) to eliminate \mathcal{Q} , and then isolating p , one obtains the general equation

$$p = \frac{k_B T}{\Omega^*} \left[\ln \left(\frac{2C_0 \Omega^* \tau_c}{k_B T \dot{\epsilon}} \right) + \ln \left(\cot(2\theta_c) + 2\theta_c - \frac{\pi}{2} \right) \right] - \frac{\epsilon_0}{\Omega^*}, \quad (56)$$

which gives the pressure once the relation $\theta_c = \theta_c(\epsilon, \dot{\epsilon}, T)$ is known from the procedure explained in the previous subsection.

Knowing $\theta_c = \theta_c(\epsilon, \dot{\epsilon}, T)$ and $p = p(\epsilon, \dot{\epsilon}, T)$, the tensile stress σ can be obtained from Eq. (37), which can be written as

$$\sigma = \frac{4\tau_c}{3 \sin(2\theta_c)} - p \quad (57)$$

or, more explicitly,

$$\sigma = \frac{4\tau_c}{3 \sin(2\theta_c)} - \frac{k_B T}{\Omega^*} \left[\ln \left(\frac{2C_0 \Omega^* \tau_c}{k_B T \dot{\epsilon}} \right) + \ln \left(\cot(2\theta_c) + 2\theta_c - \frac{\pi}{2} \right) \right] + \frac{\epsilon_0}{\Omega^*}. \quad (58)$$

The transversal compression $\sigma_x = \sigma_y$ follows from Eqs. (31).

C. The constitutive equation for $\sigma \gg \tau_c$

The procedure outlined in the preceding subsection for determining the exact dependence of the flow stress on strain, strain rate and temperature relies on solving a set of transcendental equations. However, a rather simple closed-form constitutive equation $\sigma = \sigma(\epsilon, \dot{\epsilon}, T)$ can be written if one finds acceptable to restrict the scope to the strain rates for which Eq. (44) is valid. This means $\dot{\epsilon} > 2 \times 10^{-4} \text{ s}^{-1}$ for Ti-6Al-4V, which is a typical figure of more or less general validity.

The coefficient $k_B T / (B \Omega^*)$ appearing in Eq. (52) is in general a very small adimensional quantity. As $F(\theta)$ is an universal function exhibiting large variations only close to its singularities at $\theta = 0$ and $\theta = \pi/4$, significant strains ϵ demand $\theta_c \gtrsim 0$ or $\theta_c \lesssim \pi/4$. In the latter eventuality the stress is near the minimum necessary to produce plastic flow, which progresses at a very low rate and corresponds to *creep*. The former case is the ductile deformation we are interested in.

When $\theta_c \gtrsim 0$ the universal function $F(\theta)$, given by Eq. (53), can be substituted by the asymptotic equation

$$F(\theta) = \frac{1}{\pi - 8/\pi \theta} \quad (59)$$

and then the expression (52) for the strain becomes

$$\varepsilon = \frac{1}{\pi - 8/\pi} \frac{k_B T}{B \Omega^*} \frac{1}{\theta_c} + \varepsilon_0, \quad (60)$$

where ε_0 is an integration constant determined by the condition (38). Isolating θ_c from Eq. (60) and inserting in Eqs. (56) and (57), both rewritten for $\theta_c \ll 1$, it gives

$$p = \frac{k_B T}{\Omega^*} \ln \left[\frac{(\pi - 8/\pi) C_0 (\Omega^*)^2 B \tau_c}{(k_B T)^2 \dot{\varepsilon}} (\varepsilon + \varepsilon_0) \right] - \frac{\varepsilon_0}{\Omega^*} \quad (61)$$

and

$$\sigma = \frac{2(\pi - 8/\pi)}{3} \frac{B \Omega^* \tau_c}{k_B T} (\varepsilon + \varepsilon_0) - p. \quad (62)$$

The initial condition (38), that is, $p = -\sigma_0/3$ when $\varepsilon = 0$, with σ_0 being the flow stress for $\varepsilon = 0$, allows us to put Eqs. (61) and (62) as

$$p = \frac{k_B T}{\Omega^*} \ln \left[\frac{C_0 \Omega^*}{k_B T \dot{\varepsilon}} \left(\frac{(\pi - 8/\pi) B \Omega^* \tau_c}{k_B T} \varepsilon + \sigma_0 \right) \right] - \frac{\varepsilon_0}{\Omega^*} \quad (63)$$

and

$$\begin{aligned} \sigma &= \frac{2(\pi - 8/\pi)}{3} \frac{B \Omega^* \tau_c}{k_B T} \varepsilon + \frac{2}{3} \sigma_0 \\ &- \frac{k_B T}{\Omega^*} \ln \left[\frac{C_0 \Omega^*}{k_B T \dot{\varepsilon}} \left(\frac{(\pi - 8/\pi) B \Omega^* \tau_c}{k_B T} \varepsilon + \sigma_0 \right) \right] + \frac{\varepsilon_0}{\Omega^*}, \end{aligned} \quad (64)$$

which is the general constitutive equation $\sigma = \sigma(\varepsilon, \dot{\varepsilon}, T)$ we were searching for. If one replaces in Eq. (64) $\varepsilon = 0$ and $\sigma = \sigma_0$, the approximate constitutive equation (44) for $\varepsilon = 0$ is recovered. The domain in which the approximation holds is apparent in Fig. 7, where the curves given by Eq. (44) and the exact Eq. (43) are compared.

D. Exact expression for the slope $\partial\sigma/\partial\varepsilon$ at $\varepsilon = 0$

Derivating and combining properly the equations written in subsections VI A and VI B one can deduce a closed-form equation for the slope $\partial\sigma/\partial\varepsilon$ at $\varepsilon = 0$. In general, for any ε ,

$$\begin{aligned} \frac{\partial\sigma}{\partial\varepsilon} &= B \left(\frac{4\Omega^* \tau_c}{3k_B T \cos(2\theta_c)} - \frac{1}{\cot(2\theta_c) + 2\theta_c - \pi/2} \right) \\ &\times \left[\frac{1 - \cos(2\theta_c)}{\sin(2\theta_c)} - 2\theta_c \left(1 + \frac{2}{\pi \sin(2\theta_c)} \right) \right] \\ &- \frac{2 \cos(2\theta_c)}{\pi} + \frac{\pi}{2}. \end{aligned} \quad (65)$$

For $\varepsilon = 0$ one can replace $\sin(2\theta_c) = 2\tau_c/\sigma$, and Eq. (65) becomes an expression of only the initial value of σ .

The slope $\partial\sigma/\partial\varepsilon$ at $\varepsilon = 0$ is a very important quantity because it is observed that always the maximal superplastic strain to failure is attained close to a temperature and strain rate such that

$$\left. \frac{\partial\sigma}{\partial\varepsilon} \right|_{\varepsilon=0} = 0, \quad (66)$$

which may be considered as an analytical condition for superplasticity. Although this conclusion is mostly empirical, it is quite reasonable because, as a polycrystal cannot flow steadily by the monotonic increase of the internal pressure p , Eq. (66) expresses the situation which best emulate a steady regime. The next example illustrates the point.

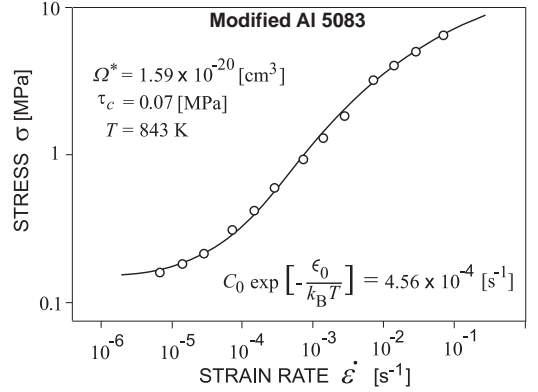


FIG. 11: The uniaxial flow stress σ for a modified Al 5083 alloy deformed at 570 °C and constant strain rate $\dot{\varepsilon}$. Circles represent the data of Kaibyshev *et. al.* (Ref. 41) and solid line depicts Eq. (43) with the material constants shown in the insets.

Fig. 11 shows the variation of flow stress with strain rate for a modified 5083 aluminium alloy, deformed at $T = 843$ K and constant true strain rate. The experimental points are due to Kaibyshev *et. al.* [41] and the solid line depicts Eq. (43) with the constants shown in the insets. These authors observed a sharp maximum in elongation to failure of 1150% for $T = 843$ K and a strain rate $\dot{\varepsilon} = 2.8 \times 10^{-3} \text{ s}^{-1}$.

Inserting in Eq. (65) the constants obtained from the fit of the stress–strain rate data, shown in Fig. 11, the slope $\partial\sigma/\partial\varepsilon$ of the stress–strain curves at $\varepsilon = 0$ can be calculated for any initial stress σ . The solid–dashed straight lines drawn in Fig. 12 represent the calculated tangents to the stress–strain curves at $\varepsilon = 0$ starting from $\sigma = 1.33, 2.4,$ and 7.0 MPa. According to Eq. (43) these three stresses correspond to the strain rates $\dot{\varepsilon} = 2.8 \times 10^{-3}, 1.4 \times 10^{-2}$ and $7.0 \times 10^{-2} \text{ s}^{-1}$. The circles in Fig. 12 represent the experimental stress–strain data taken by Kaibyshev *et. al.* at constant strain rates $\dot{\varepsilon} = 2.8 \times 10^{-3}, 1.4 \times 10^{-2}$ and $7.0 \times 10^{-2} \text{ s}^{-1}$. The consistency between theory and experiment is apparent in Fig. 12. The effective bulk modulus, which fixes the

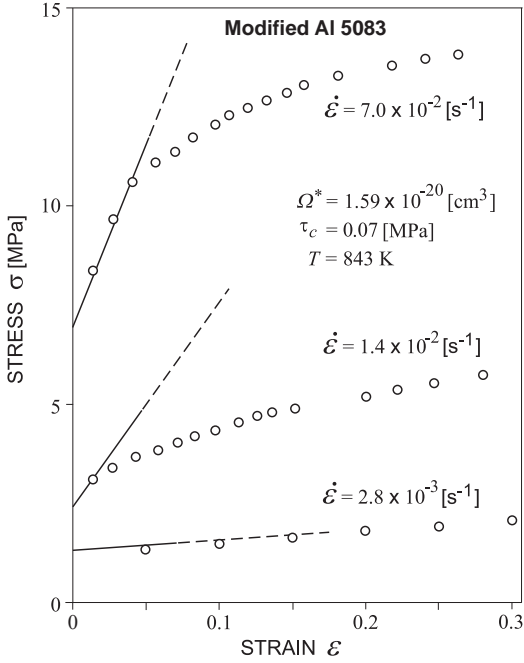


FIG. 12: Circles represent stress–strain data at constant strain rates $\dot{\epsilon} = 2.8 \times 10^{-3}$, 1.4×10^{-2} and $7.0 \times 10^{-2} \text{ s}^{-1}$ for the same system of Fig. 11. The straight lines are the tangents to the stress–strain curves at $\epsilon = 0$ and the same strain rates, calculated with Eq. (65). The effective bulk modulus is $B = 3000 \text{ MPa}$.

scale for ϵ , was taken as $B = 3000 \text{ MPa}$. Best superplastic response of the material is attained at a strain rate $\dot{\epsilon} = 2.8 \times 10^{-3}$, for which $\partial\sigma/\partial\epsilon \approx 0$ at $\epsilon = 0$.

E. Grain sliding and the sign of the concavity of the stress–strain curve

In a recently published experimental study of the plastic tensile deformation of Ti–6Al–4V, Vanderhasthen *et. al.* find out that positive concavity seems to be the fingerprint of grain boundary sliding [42, 43]. These authors conducted tests starting from room temperature to 1323 K, recording tensile properties, microstructural evolution and crystallographic texture changes at a constant true strain rate $\dot{\epsilon} = 5 \times 10^{-4} \text{ s}^{-1}$. The tests seem not intended to attain optimal superplastic performance, but clearly show a dramatic increase of the strain to fracture at $T = 873 \text{ K}$ (600° C), which reaches the optimum ($\epsilon = 1.6$) at $T = 1123 \text{ K}$ (850° C). Starting from $T = 998 \text{ K}$, grain boundary sliding begins to be dominant and, coincidentally, the corresponding stress–strain curve exhibits positive concavity over the most of the strain domain. The lower temperature range is characterized by negative concavity and grain stretching. At temperatures between $T = 1123 \text{ K}$ and $T = 1173 \text{ K}$ the stress–strain curves have positive concavity over the whole range, from

$\epsilon = 0$ to fracture at $\epsilon \approx 1.6$. For higher temperatures the strain to fracture decreases and the stress–strain curves develop a final sector with small negative curvature before failure.

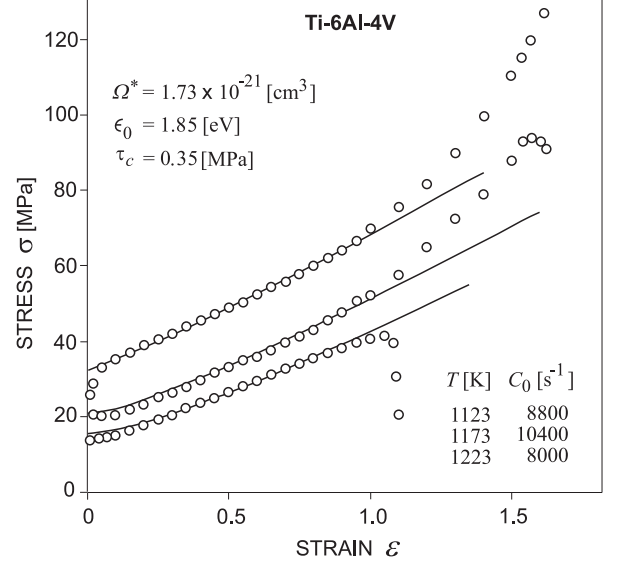


FIG. 13: Circles represent data for Ti–6Al–4V of Vanderhasthen *et. al.* at the the temperatures for which grain sliding dominates over grain stretching. Solid lines were obtained from Eq. (64) and the same set of parameters, which are shown in the insets. Just C_0 shows some variation with T , probably due to its grain size dependence. The effective bulk modulus is $B = 3000 \text{ MPa}$.

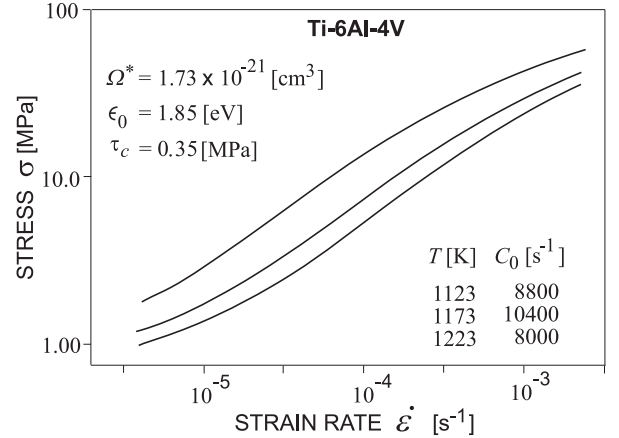


FIG. 14: Stress–strain rate curves calculated from Eq. (43) and the same material constants of Fig. 13. No experimental data are available to compare with.

The open circles in Fig. 13 represent experimental data taken by Vanderhasthen *et. al.* on the stress–strain response of the titanium alloy Ti–6Al–4V at the three temperatures for which the deformation is observed to take

place by grain sliding [42, 43]. The strain rate was kept at $\dot{\epsilon} = 5.0 \times 10^{-4} \text{ s}^{-1}$ in all runs. The samples exhibit high ductility but not properly superplasticity. The solid lines represent the asymptotic expression (64) for the three temperatures, with the parameters shown in the insets and $B = 3000 \text{ MPa}$. Eq. (64) can describe with high precision the experimental situation, which can be shown by comparing the values for σ at $\epsilon = 0$ given by Eq. (64) with the exact value σ_0 , obtained from Eq. (43) to introduce it into the same Eq. (64) as a one of its constants. The agreement between theory and experiment is remarkable up to $\epsilon = 1$.

Fig. 14 shows the stress–strain rate curves given by Eq. (43) and the same material constants used to fit the data of Fig. 13. There is no experimental points to compare with since Vanderhasten *et. al.* employed a unique strain rate. The curves exhibit the typical sigmoidal shape.

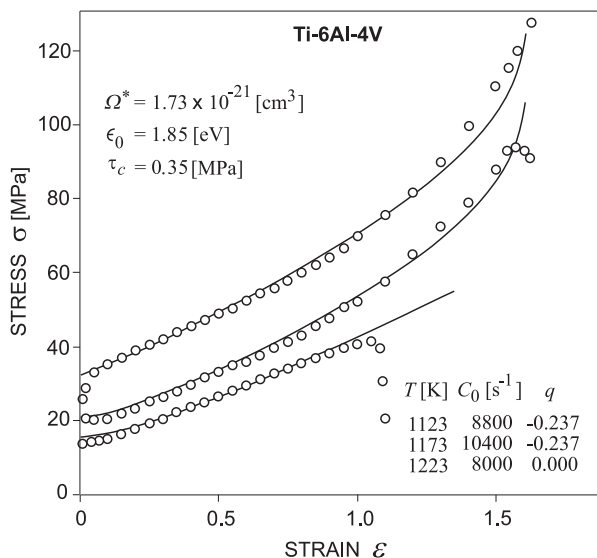


FIG. 15: Same as Fig. 13, but with C_0 replaced by C'_0 , as given by Eq. (67) with the values of q shown in the inset. C'_0 models the effect of grain size variations.

In general, C_0 depends on the grain size d as d^{-3} and the rest of the parameters do not vary with d [22]. Fig. 15 shows an attempt to explain the departure between theory and experiment, starting at $\epsilon = 1$, by the dynamic modification of the grain size. The curves represent Eq. (64) with C_0 substituted by

$$C'_0 = (1 + q\epsilon^3)C_0, \quad (67)$$

where q is a constant. The values of q giving the best fit to experiment are shown in one of the insets of Fig. 15. Amazingly, q turns out to be such that $C'_0 = 0$ at the fracture strain. This means that failure occurs because the grains become unable to slide, which can hardly be explained by just their size variations. The explanation

may be as follows: The mean grain sizes measured by Vanderhasten *et. al.* at 1123 and 1173 K show a rather irregular reduction on strain. The consequent division of old grains involves the creation of new grain surfaces which do not have necessarily the composition and structure of the old ones. Grain boundaries are efficient traps for impurities, and can condense atomic species having a low bulk concentration. However, the process is governed by bulk diffusion and is not rapid. Therefore, concerning their composition and consequent sliding ability, fresh grains may be very different than well-aged ones. From this viewpoint, grain size variations may simply reduce the number of grains able to slide. This explains also why the smooth stress–strain curves do not reflect the irregularities observed in the grain size–strain curves.

The theoretical approach to finite strain superplasticity put forward here permits to explain quantitatively the main features observed in the superplastic deformation. However, the theory lacks an important element: the effect of heat generation at the sliding grain boundaries. In our scheme, the whole work made by the external forces is dissipated into heat at the sliding grain boundaries, which occupy a very small volume when compared with the grain bulk. Hence one may expect that grain boundaries will be at a higher temperature than bulk matter, being the nominal temperature the bulk one. Grain boundaries whose normals are within solid angles, determined by θ_c , around the principal stress directions do not slide because the in-plane shear stress is smaller than τ_c , and then remain at the bulk temperature. Bending downward of the stress–strain curves at high strains and strain rates seems to be a grain boundary temperature effect.

F. Two phase alloys and the nature of the superplastic deformation

The scheme described thus far should hold for single phase alloys. Materials combining two or more allotropic phases in thermodynamic equilibrium may display a more complex phenomenology. In particular, superplastic materials are generally two-phase or pseudo single phase alloys. Probably the most characteristic example of the former is Ti-6Al-4V, which combines an α hcp solid phase with a β phase with bcc structure, in comparable volume fractions up to the β transus temperature. Cope *et al.* [3, 10] observed best superplastic response of Ti-6Al-4V for a temperature $T = 1153 \text{ K}$, for which the β phase proportion was 0.42%. In pseudo single phase materials the second phase occurs as small inclusions between the grains constituting the main one.

The new feature introduced by the coexistence of two allotropic phases in thermodynamical equilibrium is that a volume reduction is not necessarily related with just the elastic properties of the material. If the two phases (which we will call generically as α and β) have different specific volumes, the total volume may change also by the

transformation of part of one of the phases into the other one. In general, the atomic fraction of, for instance, the β phase

$$\frac{N_\beta}{N} = \eta_\beta(T, p), \quad (68)$$

where N_β is the number of atoms of the main constituent of the alloy in the β phase and $N = N_\alpha + N_\beta$ is the total, is a function of the temperature T and pressure p . If p changes with time, the atomic fraction of the phases changes, as well as the total volume V . Hence, the dilation rate is no more given by Eq. (33) but by

$$\frac{\dot{V}}{V} = \left[-\frac{1}{B} + \frac{v_\beta - v_\alpha}{N_\alpha v_\alpha + N_\beta v_\beta} \left(\frac{\partial N_\beta}{\partial p} \right)_T \right] \dot{p}, \quad (69)$$

where v_α and v_β are the volume per atom of the two phases.

Eq. (69) assumes that the atomic fractions have their equilibrium values in any instant, and hence a quasi-static process, otherwise the transformation kinetics would come into the fore. The total area of the interfaces between the phases is maximal when their volumes have the same value, and then comparable volume fractions contribute to increase the phase transformation rates, and the accuracy of Eq. (69). Also, the new isothermal coefficient appearing in Eq. (69) is in general not a constant, and it is expected to be much more sensitive to temperature than $1/B$. With this in mind we define

$$\frac{1}{B_{\alpha\beta}} = -\frac{v_\beta - v_\alpha}{N_\alpha v_\alpha + N_\beta v_\beta} \left(\frac{\partial N_\beta}{\partial p} \right)_T \quad (70)$$

and call

$$\frac{1}{B^*} = \frac{1}{B} + \frac{1}{B_{\alpha\beta}}. \quad (71)$$

$B_{\alpha\beta}$ is a positive quantity since the two factors in the right hand side of Eq. (70) have opposite signs, as demanded by mechanical stability.

The equations of the previous sections are formally recovered this way, with an effective bulk modulus B^* instead of the purely elastic one B .

The elastic modulus B takes in general large values (typically $B \approx 1 \times 10^5$ MPa for metals), which is not necessarily the case of $B_{\alpha\beta}$. For two phases coexisting in thermodynamical equilibrium one may expect that the volume fraction of each one would vary significantly for pressure variations much smaller than the yield stress. Then, values of less than 1 MPa for $B_{\alpha\beta}$ are quite reasonable. In such a situation $1/B \ll 1/B_{\alpha\beta}$ and $1/B^*$ is several orders of magnitude larger than $1/B$. By this reason solids exhibiting two allotropic phases in equilibrium may display a special plastic behaviour, of which superplasticity seems to be an example.

The abnormally large strains to failure displayed by superplastic materials have been attributed to the better stability they have against necking in tensile tests. The plastic flow can be represented by the relation

$$\sigma = K \dot{\epsilon}^m, \quad (72)$$

where m is a function of $\dot{\epsilon}$ and ϵ , generally known as the strain rate sensitivity, which is always smaller than unity. When $m = 1$ any irregularity in the cross section of the sample is not accentuated by the deformation in a tensile test, necking has no effect and the material behaves as a Newtonian viscous fluid. Necking instability is high for m below 0.5 and decreases markedly when $m \geq 0.5$. Indeed, the condition of high values of m is a necessary requirement, but not enough to reach elongations as large as those termed superplastic. Our previous discussions show that plastic elongation has a limit because demands a volume reduction, and failure is not a matter of just a mechanical instability of geometric origin.

Therefore, in our view, superplasticity has its real origin in three concurrent features of the material and physical conditions of the deformation process: (a) A high strain sensitivity m . (b) The ability of the material to reduce the internal pressure p by undergoing a phase transformation to a phase of higher density. (c) The material must be in the verge of a ductile to brittle transition. This latter requirement is explained below, taking the superplastic behaviour of titanium Ti-6Al-4V to illustrate the argument.

G. The high temperature second yield point

The general properties of the stress *vs.* strain curves can be visualized from just examining Eq. (64) for the strain dependent flow stress σ . It has a first term linear in ϵ , with slope proportional to $1/T$, and a negative logarithmic term whose coefficient increases with T . Hence, at low temperatures σ is linear in ϵ and, as T increases, the slope decreases and the function develops positive concavity. Beyond a critical temperature for which the slope at the origin vanishes the curve starts at $\epsilon = 0$ with negative slope and, after surpassing a minimum, or second yield point, begins to increase monotonically.

Hence, Eq. (64) predicts strain hardening at any strain for temperatures below a critical temperature, which roughly coincides with the temperature which optimizes superplastic properties. At higher temperatures the material should weaken for strains between $\epsilon = 0$ and the second yield point. This configures a mechanically unstable situation which cannot occur in practice in a smooth and homogeneous way. The equations written so far describe the mechanical response at a point, which does not necessarily can be straightforwardly extended to the whole sample. Homogeneity is a quite reasonable assumption to study averaged properties in the macroscopic scale, but may fail in critical situations. We can

safely assume that Ω^* and ϵ_0 are uniform and constant throughout the material, but C_0 depends on the grain size as d^{-3} [22], and hence may fluctuate or have a multimodal distribution, following grain size.

There is a class of mild steels [44] and aluminium alloys [45, 46] exhibiting stress-strain curves with two yield points. The plastic deformation of these materials is inhomogeneous and takes place by a series of successive sudden band formations (Lüders bands [47]), transversal to the tensile axis and making a rather precise angle with it (of about 56°), which concentrate the strain. The flow stress keeps constant (though displaying a serrated aspect) until the bands, increasing in number and extension, fill the whole sample and the complete material becomes strained beyond the second yield point strain. Just then the stress starts to increase. In the intermediate steps, samples have sections with no strain and sections strained beyond the second yield strain. The relevant question is then how a system with the stress-strain curves given by Eq. (64) will evolve with strain, and what kind of effective stress-strain curves could be expected from such evolution.

If our material is not exactly homogeneous the critical temperature for the onset of the second yield point is not the same in its whole extension. Hence, at temperatures close to these critical temperatures and small strain one may expect the solid will be partitioned in a network

of sectors hardening on strain, and another one which weakens. As the stress is uniform, the weakening sectors will deform much faster, and will be responsible for the main part of the effective strain before reaching their second yield point. Meanwhile the hardening sectors will furnish mechanical stability against sudden yield steps, like Lüders band generation.

Anyway, the condition for superplastic behaviour seems related with the onset of the second yield point, producing a transition to a potentially unstable system. Such a transition begins at the temperature for which $\partial\sigma/\partial\epsilon$ at $\epsilon = 0$ vanishes and changes from positive to negative sign. On the other hand, generally speaking, the most basic condition for a steady flow, as superplastic deformation tends to be, is that the dynamical variables remain constant and independent of ϵ , which here represents time. As σ varies with ϵ , all what can be done is to emulate a steady flow by providing the conditions that keep $\partial\sigma/\partial\epsilon$ small and steady in a range as large as possible, which incorporates $\epsilon = 0$.

Acknowledgments

The authors thanks the support by the Programa Bicentenario de Ciencia y Tecnología (Chile) ACT-26.

-
- [1] J. Pilling and N. Ridley, *Superplasticity in crystalline solids*, (The Institute of Metals, Camelot, Southampton, UK, 1989).
 - [2] T. G. Nieh, J. Wadsworth and O. D. Sherby, *Superplasticity in metals and ceramics* (Cambridge, UK 1997).
 - [3] M. T. Cope and N. Ridley, *Mat. Sci. Technol.* **2**, 140 (1986).
 - [4] T. H. Thomsen, D. L. Holt and W. A. Backofen, *Met. Eng. Quart.* **2**, 1 (1970).
 - [5] *Aerospace Materials*, edited by B. Cantor, H. Assender and P. Grant. (Institute of Physics Publishing, Bristol, UK, 2001).
 - [6] M. A. Khaleel, H. M. Zbib and E. A. Nyberg, *Int. J. Plast.* **17**, 277 (2001).
 - [7] M. B. Taylor, H. M. Zbib and M. A. Khaleel, *Int. J. Plast.* **18**, 415 (2002).
 - [8] D. W. Livesey and N. Ridley, *Metall. Trans.* **9A**, 519 (1978).
 - [9] D. W. Livesey and N. Ridley, *Metall. Trans.* **13A**, 1619 (1982).
 - [10] M. T. Cope, D. R. Evetts and N. Ridley, *J. Mat. Sci.* **21**, 4003 (1986).
 - [11] A. Ball and M. M. Hutchinson, *Met. Sci. J.* **3**, 1, (1969).
 - [12] A. K. Mukherjee, *Mater. Sci. Eng.* **8**, 83 (1971).
 - [13] T. G. Langdon, *Phil. Mag.*, **22A**, 689 (1970).
 - [14] H. W. Hayden, S. Floreen and P. D. Goodall, *Metall. Trans.* **3A**, 833 (1972).
 - [15] M. F. Ashby and R. A. Verrall, *Acta Metall.* **21**, 149 (1973).
 - [16] R. C. Gifkins, *Metall. Trans.* **7A**, 1225 (1976).
 - [17] A. Arieli and A. K. Mukherjee, *Mater. Sci. Eng.* **45**, 61 (1980).
 - [18] H. Fukuyo, H. C. Tsai, T. Oyama and O. D. Sherby, *ISIJ International* **31**, 76 (1991).
 - [19] C. G. Wang, M. W. Fu, C. X. Cao and H. B. Dong, *Mat. Sci. Eng. A*, in press.
 - [20] M. Lagos and H. Duque, *Int. J. Plast.* **17**, 369 (2001).
 - [21] M. Lagos, *Phys. Rev. Lett.* **85**, 2332 (2000).
 - [22] M. Lagos, *Phys. Rev. B* **71**, 224117 (2005).
 - [23] M. Lagos, *Phys. Rev. B* **73**, 224107 (2006).
 - [24] P. Bellon and R. S. Averback, *Phys. Rev. Lett.* **74**, 1819 (1995).
 - [25] D. J. Srolovitz, *Acta Metall.* **37**, 621 (1989).
 - [26] J. Müller and M. Grant, *Phys. Rev. Lett.* **82**, 1736 (1999).
 - [27] M. A. Grinfeld, *Dokl. Acad. Nauk. SSSR* **265**, 836 (1982); *Sov. Phys. Dokl.* **31**, 831 (1986); *Europhys. Lett.* **22**, 723 (1993).
 - [28] D. R. M. Williams, *Phys. Rev. Lett.* **75**, 453 (1995).
 - [29] F. Y. Génin, *J. Appl. Phys.* **77**, 5130 (1995).
 - [30] D. E. Jones, J. P. Pelz, Y. Hong, E. Bauer and I. S. T. Tsong, *Phys. Rev. Lett.* **77**, 330 (1996).
 - [31] D. E. Jesson, K. M. Chen, S. J. Pennycook, T. Thundat and R. J. Warmack, *Phys. Rev. Lett.* **77**, 1330 (1996).
 - [32] P. C. Searson, R. Li and K. Sieradzki, *Phys. Rev. Lett.* **74**, 1395 (1995).
 - [33] R. Q. Hwang, J. C. Hamilton, J. L. Stevens and S. M. Foiles, *Phys. Rev. Lett.* **75**, 4242 (1995).
 - [34] R. Raj and M. F. Ashby, *Metall. Trans.* **2**, 1113 (1971).
 - [35] Y. J. Wei and L. Anand, *J. Mech. Phys. Sol.* **52**, 2587 (2004).

- [36] J. S. Vetrano, E. P. Simonen and S. M. Bruemmer, *Acta Mater.* **47**, 4125 (1999).
- [37] J. S. Vetrano, C. H. Henager and E. P. Simonen, in *Superplasticity – Current Status and Future Potential*, edited by P. B. Berbon, M. Z. Berbon, T. Sakuma and T. Langdon. (Materials Research Society, Warrendale, PA, 2000).
- [38] C. H. Hamilton, C. C. Bampton and N. E. Paton in *Superplastic Forming in Structural Alloys*, edited by N. E. Paton and C. H. Hamilton. (The Metallurgical Society of AIME, Warrendale, PA, 1982).
- [39] J. Pilling and N. Ridley, in *Aluminium Technology '86*, edited by T. Sheppard. (Institute of Metals, London, UK, 1986)
- [40] M. T. Cope, M. Sci. Thesis, Victoria University of Manchester, U. K. (1982).
- [41] R. Kaibyshev, F. Musin, D. R. Lesuer and T. G. Nieh, *Mater. Sci. and Eng. A* **342**, 169 (2003).
- [42] M. Vanderhasten, L. Rabet and B. Verlinden, *J. Mat. Eng. Performance* **16**, 208 (2007).
- [43] M. Vanderhasten, L. Rabet and B. Verlinden, *Materials and Design* **29**, 1090 (2008).
- [44] R. Song, D. Ponge and D. Raabe, *Acta Mater.* **53**, 4881 (2005).
- [45] J. S. Hayes, R. Keyte and P. B. Prangnell, *Mater. Sci. and Technol.* **16**, 1259 (2000).
- [46] Z. C. Wang and P. B. Prangnell, *Mater. Sci. and Eng. A* **328**, 87 (2002).
- [47] R. Hutanu, L. Clapham and R. B. Rogge, *Acta Mater.* **53**, 3517 (2005).